Supplement of Atmos. Chem. Phys., 15, 8301–8313, 2015
http://www.atmos-chem-phys.net/15/8301/2015/
doi:10.5194/acp-15-8301-2015-supplement

Atmospheric Chemistry and Physics Open Access

Supplement of

Formation and aging of secondary organic aerosol from toluene: changes in chemical composition, volatility, and hygroscopicity

L. Hildebrandt Ruiz et al.

Correspondence to: L. Hildebrandt Ruiz (lhr@che.utexas.edu)

S1 Modification of Standard Fragmentation Table

Several adjustments were made to the standard fragmentation table (Allan et al., 2004) for the analysis of HR and UMR data. Most importantly, a significant adjustment was made to the treatment of water fragmentation (Section S1.2) and to the fraction of observed H_2O attributed to organics (Section S1.3).

S1.1 Air Fragmentation

The fragmentation pattern of air at *m/z* 44 (CO_2^+), *m/z* 29 ($N^{15}N^+$), *m/z* 18 (H_2O^+) and *m/z* 16 (O^+) was calculated using difference spectra (signal – background) at UMR during filter measurements, which were taken at the beginning (before aerosol formation) and at the end of every experiment. H_2O^+, $N^{15}N^+$ and CO_2^+ were calculated as constant fractions of the N_2^+ signal at *m/z* 28. O^+ was calculated as a constant fraction of N^+. When the fractions were different at the beginning and end of the experiments, a linear function was used to approximate the time-dependent fraction throughout the experiment. In all cases the calculated fractions did not differ greatly from the standard values.

S1.2 Water Fragmentation

Water dominates the signal in the background (closed) spectrum at *m/z* 16 (O^+), *m/z* 17 (HO^+) and *m/z* 18 (H_2O^+). It is standard practice to determine the water fragmentation pattern from linear regressions to the closed signal of *m/z* 16 vs. *m/z* 18 and *m/z* 17 vs. *m/z* 18. In this way the O^+/H_2O^+ and HO^+/H_2O^+ ratios were determined for each experiment; the values, summarized in Table S1, differ slightly from the default values of 4% and 25% for O^+/H_2O^+ and HO^+/H_2O^+, respectively. However, this treatment of water fragmentation does not account for the H-atoms which were bound to HO^+ and O^+ before fragmentation. Therefore, H was added to the standard fragmentation table to obtain an H:O ratio of 2 in the total signal of H_2O determined by AMS data analysis (Canagaratna et al., 2015). This addition of H is made in three locations in the fragmentation table (water, organics and sulfate) because observed particle-phase H_2O is divided between these species. The resulting changes in mass of water, organics and sulfate are low due to the low atomic weight of H. But, the addition of H changes the organic H:C ratio calculated in

elemental analysis of the organic aerosol (OA) and therefore the average carbon oxidation state (OS_c) estimated from O:C and H:C ratios ($OS_c \sim 2\times O:C - H:C$) (Kroll et al., 2011).

S1.3 Organic Fragmentation

Important changes were also made to the organic fragmentation table. Based on the recommendation by Aiken et al. (2008), the following fragmentation pattern should be used relative to the *m/z* 44 (or CO_2^+ for HR analysis) signal: *m/z* 28 (CO^+) = 100%, *m/z* 18 (H_2O^+) = 22.5%. Since the experiments presented here contained isotopically labeled species, organic H_2O^+ was instead set as a function of the ($^{13}CO_2^+ + CO_2^+$) signal. When using 22.5%, the mass attributed to particulate water correlated with organic mass during the experiment, which is unexpected in these dry experiments (RH was less than 10%). There may be some water in the particles if the ammonium sulfate seed particles were not dried completely; however, the particle-phase water signal should not correlate with total organic signal. Thus, the ratio of organic H_2O^+ to $^{13}CO_2^+ + CO_2^+$ was chosen so that the mass of water does not correlate with the mass of organics ($R < 0.01$). The ratios of organic H_2O^+ to ($^{13}CO_2^+ + CO_2^+$) are provided in Table 2 and ranged from 0.3 to 2.4, higher than the ratio of 0.225 in the default fragmentation table. Calibration experiments suggest that polyacids, diacids and multifunctional organic molecules have H_2O^+/CO_2^+ ratios of 1, 2 and 0.5-1.5, respectively when analyzed with the AMS, and polyols have H_2O^+/CO_2^+ exceeding 10 (Canagaratna et al., 2015). Thus, the observation of high H_2O^+/CO_2^+ in these experiments may point to an importance of these functional groups in the OA produced. Increasing the amount of organic H_2O significantly increased organic mass as well as O:C in these experiments; it does not increase the approximated oxidation state.

A relative ionization efficiency (RIE) of 2.0 was used for all H_2O including the organic H_2O. This RIE is the ionization efficiency which has been determined for H_2O (Mensah et al., 2011) and is correct to use for the H_2O fragments from dehydration of organics if and only if H_2O ionizes after fragmentation. If the organic molecule is ionized and then dehydrates and results in H_2O^+, an RIE of 1.4 should be used (the RIE of organics). The only place where this uncertainty (whether fragmentation follows or precedes ionization) affects the presented results is in the calculated ratios of $H_2O^+/(^{13}CO_2^+ + CO_2^+)$ presented in Table 2; these ratios would be higher by a factor of (2.0/1.4) if dehydration follows ionization. The ratio of $^{13}CO^+$ to $^{13}CO_2^+$ was close to 1

throughout the experiments (Table 2 in main manuscript), so the ratio CO^+/CO_2^+ =1 from the standard fragmentation table was used.

S1.4 Treatment of NO^+ and NO_2^+

In these experiments, no inorganic nitrate is introduced or anticipated. Hence the ions assigned to the nitrate family in the HR analysis (NO^+, NO_2^+) are presumed to be due to organic nitrates and were added to the total organic aerosol mass in the HR batch table. The relative ionization efficiency (RIE) of 1.0 is used to quantify the contribution from these fragments. The elemental analysis examines the oxidation state of the carbon atoms; hence, nitrate fragments (NO^+, NO_2^+) were **not** included in the calculation of O:C and H:C.

S2 Quantification of AMS Data

S2.1 Ionization efficiency, airbeam and V vs W modes

Data were corrected for changes in the instrument airbeam (AB) over the course of an experiment. The ionization efficiency (IE) for each experiment was adjusted based on the ratio of the AB during the experiment to the AB during the ionization efficiency calibration conducted before this set of experiments was started (calibration IE/AB = 4.65×10^{-13}). Data were corrected for changes in the instrument airbeam (AB) over the course of an experiment. The ionization efficiency (IE) for each experiment was adjusted based on the ratio of the AB during the experiment to the AB during the ionization efficiency calibration conducted before this set of experiments was started (calibration IE/AB = 4.65×10^{-13}). Total aerosol concentrations were calculated in the following way to exploit the higher sensitivity (and accuracy) in V-mode and the higher resolution in W-mode. First, UMR fragmentation and batch tables were used to obtain bulk concentration data for sulfate in V and W mode. The V/W ratio was then computed for sulfate, obtaining a measure of the difference in total concentrations measured in these two modes. Second, HR analysis and the HR fragmentation and batch tables were used to obtain organic and sulfate concentrations in W-mode. The W-mode HR data were then multiplied by the (V/W) ratio (from UMR analysis) to obtain the most quantitative estimate of the amount of organic and sulfate mass detected by the AMS. Because all sulfate in these experiments is from the ammonium sulfate seed particles, sulfate mass was multiplied by 1.375 to obtain ammonium

sulfate mass. Using the V/W ratio as a correction factor indirectly applies an AB correction in W-mode. When sulfate data were not available, nitrate concentrations in V and W mode were used instead to compute the V/W ratio. The AB and V/W ratio used to correct the data in each experiment are shown in Table S1.

S2.2 Determination of collection efficiency

A further issue with all AMS analysis is that the AMS does not detect all sampled particles, primarily due to particle bounce at the vaporizer. The AMS collection efficiency (CE) for these data was estimated by matching AMS mass distributions and SMPS volume distributions using the OA density (ρ_{org}) and AMS CE as fitting parameters, with the algorithm developed by Kostenidou et al. (2007) . Particle time of flight (pToF) distributions of organics and sulfate (SO_4^{2-}) from V-mode were used but scaled by the adjusted HR aerosol masses (from MS mode) obtained as described above. The pToF distributions were smoothed before fitting using a 19-point, 2nd order Savitzky-Golay smoothing.

The data from each experiment were split according to whether the OA had been passed through the bypass or the TD to observe whether the denuded OA had a different CE and/or density compared to the total OA. The data from Expt. 9 were further split into a total of 16 periods to explore variation in CE and OA density over the course of an experiment (e.g. with increasing OH exposure of the OA or different denuder temperatures). As can be seen in Fig S1, the CE and OA density did not change significantly over the course of an experiment. There is also very little difference in CE between the OA passed through the bypass or the thermodenuder (Table S1, all experiments). As observed earlier (Lee et al., 2010) the algorithm for estimating AMS CE and OA density is much less sensitive to the OA density than to the AMS CE, and the estimated CE essentially remains the same after fixing the OA density at 1.5 g cm^{-3} (Fig S1). The values of CE are used to correct OA concentrations for the calculation of OA mass yield and mass fraction remaining. The values of OA density shown in Table S1 are used to convert aerodynamic to mobility diameter for CCN analysis.

References:

Aiken, A. C., DeCarlo, P. F., Kroll, J. H., Worsnop, D. R., Huffman, J. A., Docherty, K., Ulbrich, I. M., Mohr, C., Kimmel, J. R., Sueper, D., Sun, Y., Zhang, Q., Trimborn, A. M., Northway, M. J., Ziemann, P. J., Canagaratna, M. R., Alfarra, M. R., Prevot, A. S. H., Dommen, J., Duplissy, J., Metzger, A., Baltensperger, U. and Jimenez, J. L.: O/C and OM/OC Ratios of Primary, Secondary, and Ambient Organic Aerosols with High Resolution Time-of-Flight Aerosol Mass Spectrometry, Environ. Sci. Technol., 42, 4478–4485, 2008.

Allan, J. D., Delia, A. E., Coe, H., Bower, K. N., Alfarra, M. R., Jimenez, J. L., Middlebrook, A. M., Drewnick, F., Onasch, T. B., Canagaratna, M. R., Jayne, J. T. and Worsnop, D. R.: A generalised method for the extraction of chemically resolved mass spectra from Aerodyne aerosol mass spectrometer data, J. Aerosol Sci., 35(7), 909–922, doi:10.1016/j.jaerosci.2004.02.007, 2004.

Canagaratna, M. R., Jimenez, J.-L., Kroll, J. H., Chen, Q., Kessler, S. H., Massoli, P., Hildebrandt Ruiz, L., Fortner, E., Williams, L., Wilson, K., Surratt, J. D., Donahue, N. M., Jayne, J. T. and Worsnop, D. R.: Elemental Ratio Measurements of Organic Compounds using Aerosol Mass Spectrometry: Characterization, Improved Calibration, and Implications, Atmos. Chem. Phys., 15, 253–272, 2015.

Kostenidou, E., Pathak, R. K. and Pandis, S. N.: An Algorithm for the Calculation of Secondary Organic Aerosol Density Combining AMS and SMPS Data, Aerosol Sci. Technol., 41(11), 1002–1010, doi:10.1080/02786820701666270, 2007.

Kroll, J. H., Donahue, N. M., Jimenez, J. L., Kessler, S. H., Canagaratna, M. R., Wilson, K. R., Altieri, K. E., Mazzoleni, L. R., Wozniak, A. S., Bluhm, H., Mysak, E. R., Smith, J. D., Kolb, C. E. and Worsnop, D. R.: Carbon oxidation state as a metric for describing the chemistry of atmospheric organic aerosol, Nat. Chem., 3, 133–139, 2011.

Lee, B.-H., Hildebrandt, L., Kostenidou, E., Riipinen, I., Engelhart, G. J., Donahue, N. M. and Pandis, S. N.: Volatility of organic aerosol sampled during FAME-2008, Atmos. Chem. Phys., 10, 12149–12160, 2010.

Mensah, A. a., Buchholz, A., Mentel, T. F., Tillmann, R. and Kiendler-Scharr, A.: Aerosol mass spectrometric measurements of stable crystal hydrates of oxalates and inferred relative ionization efficiency of water, J. Aerosol Sci., 42(1), 11–19, doi:10.1016/j.jaerosci.2010.10.003, 2011.

Table S1. Details on AMS data analysis

Expt #	O/H_2O	HO/H_2O	AB ($\times 10^5$)	Org < 106 ratio	v/w	CE_{BP}	CE_{TD}	$\rho_{org,BP}$	$\rho_{org,TD}$
1	0.027	0.229	5.28	0.966	0.427	0.20	0.20	1.275	1.400
2	0.017	0.232	5.36	0.977	0.478	0.35	0.30	1.350	1.400
3	0.028	0.223	5.33	0.959	0.466	0.25	0.25	1.375	1.425
4	0.020	0.238	5.48	0.970	0.490	0.25	0.25	1.350	1.450
5	0.016	0.234	5.04	0.959	0.504	0.30	0.30	1.325	1.375
6	0.042	0.238	5.09	0.961	0.531	0.25	0.25	1.275	1.375
7	0.036	0.269	4.84	0.971	0.490	0.25	0.25	1.375	1.475
8	0.037	0.227	4.80	0.968	0.504	0.20	0.20	1.325	1.400
9	0.022	0.234	5.05	0.974	0.705	0.40	0.35	1.425	1.400

Table S2. Evaporation model inputs for each experiment

Expt.	Diameter[a] (nm)	Concentration[b] ($\mu g\ m^{-3}$)	OA Density ($kg\ m^{-3}$)
1	298	42.8	1.28
2	234	6.4	1.35
3	275	51.4	1.38
4	228	26.0	1.35
5	234	11.8	1.33
6	243	94.4	1.28
7	285	41.5	1.38
8	266	30.1	1.33
9	251	22.8	1.43

[a]Average volumetric mode diameter of the bypass line.

[b]Average CE corrected concentration of the bypass line .

Tables S3 and S4: Enthalpy of Vaporization and Accommodation Coefficient Sensitivity Analysis

Table S3**.** Normalized shifting factors for all tested values of ΔH_{vap}

Normalized Shifting Factors			
Expt	**ΔH_{vap} = 20 kJ**	**ΔH_{vap} = 80 kJ**	**ΔH_{vap} = 120 kJ**
1	0.36	0.31	0.29
2	0.08	0.04	0.01
3	0.57	0.31	0.16*
4	0.50	0.25	0.27*
5	0.74*	0.52	0.57
6	0.93	0.53	0.61*
7	1.0	1.00	1.00*
8	0.38*	0.23	0.13
9	0.22*	0.14	0.07

* The sum of squared residuals exceeding 0.10

Table S4. Shifting factors and SSR values for the most volatile (Expt. 7) and least volatile (Expt. 9) experiments in our dataset estimated using different values of accommodation coefficient.

α_m	**Shifting Factors**			**Sum of the Squared Residuals**	
	Expt 7	Expt 9	Ratio (Expt 7 / Expt 9)	Expt 7	Expt 9
0.01	1.95	0.32	6.14	0.09	0.079
0.1	0.21	0.03	6.24	0.09	0.078
1.0	0.04	0.006	7.04	0.10	0.075

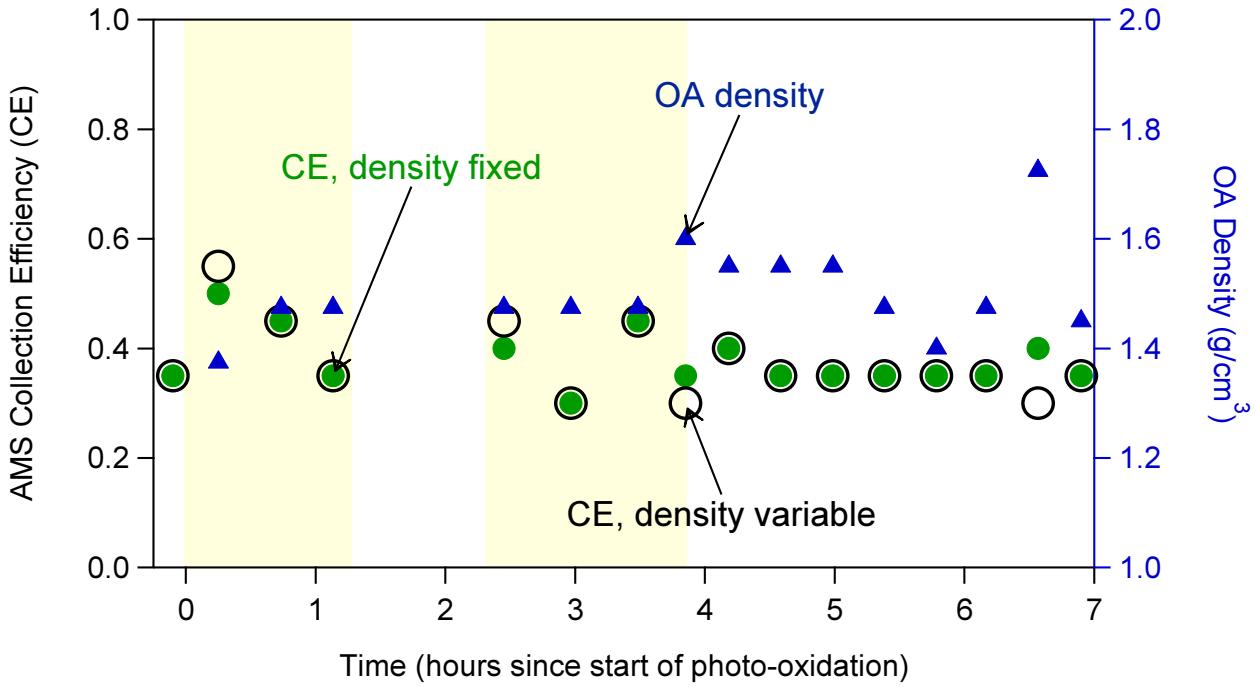

Figure S1. Estimated CE (solid green and open black circles) and OA density did not change much over the course of an experiment (shown here are the data for Expt. 9). The algorithm used is not as sensitive to OA density, and fixing the density at 1.5 g cm^{-3} changes the CE values only slightly for some, and not at all for other time periods.

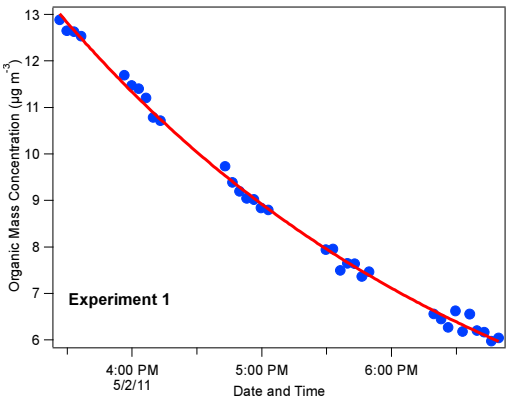
Organic Mass Concentration (µg m-3)
Experiment 1
4:00 PM
5/2/11
5:00 PM
6:00 PM
Date and Time

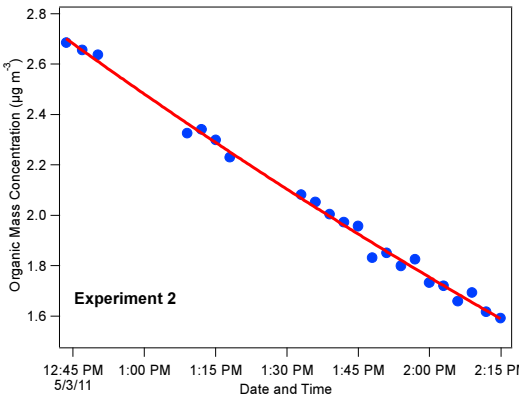
Organic Mass Concentration (µg m-3)
Experiment 2
12:45 PM
5/3/11
1:00 PM
1:15 PM
1:30 PM
1:45 PM
2:00 PM
Date and Time

1

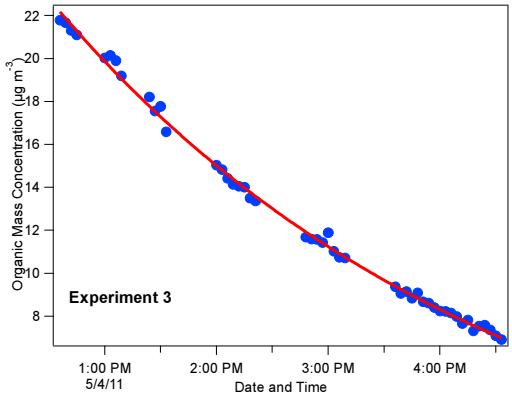
Organic Mass Concentration (µg m-3)
Experiment 3
1:00 PM
5/4/11
2:00 PM
3:00 PM
4:00 PM
Date and Time

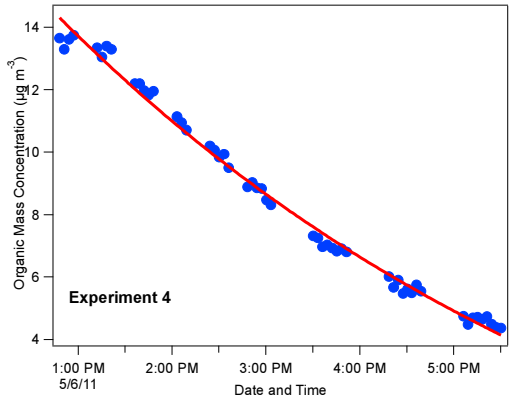
Organic Mass Concentration (µg m-3)
Experiment 4
1:00 PM
5/6/11
2:00 PM
3:00 PM
4:00 PM
5:00 PM
Date and Time

2

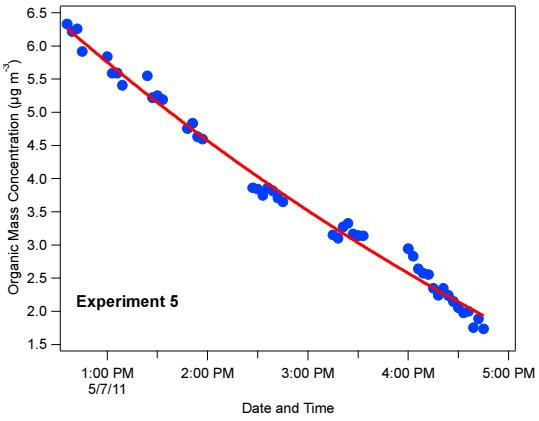
Organic Mass Concentration (µg m-3)
Experiment 5
1:00 PM
5/7/11
2:00 PM
3:00 PM
4:00 PM
5:00 PM
Date and Time

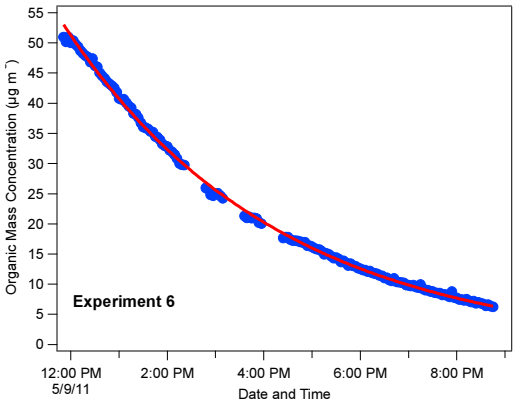
Organic Mass Concentration (µg m-3)
Experiment 6
12:00 PM
5/9/11
2:00 PM
4:00 PM
6:00 PM
8:00 PM
Date and Time

3

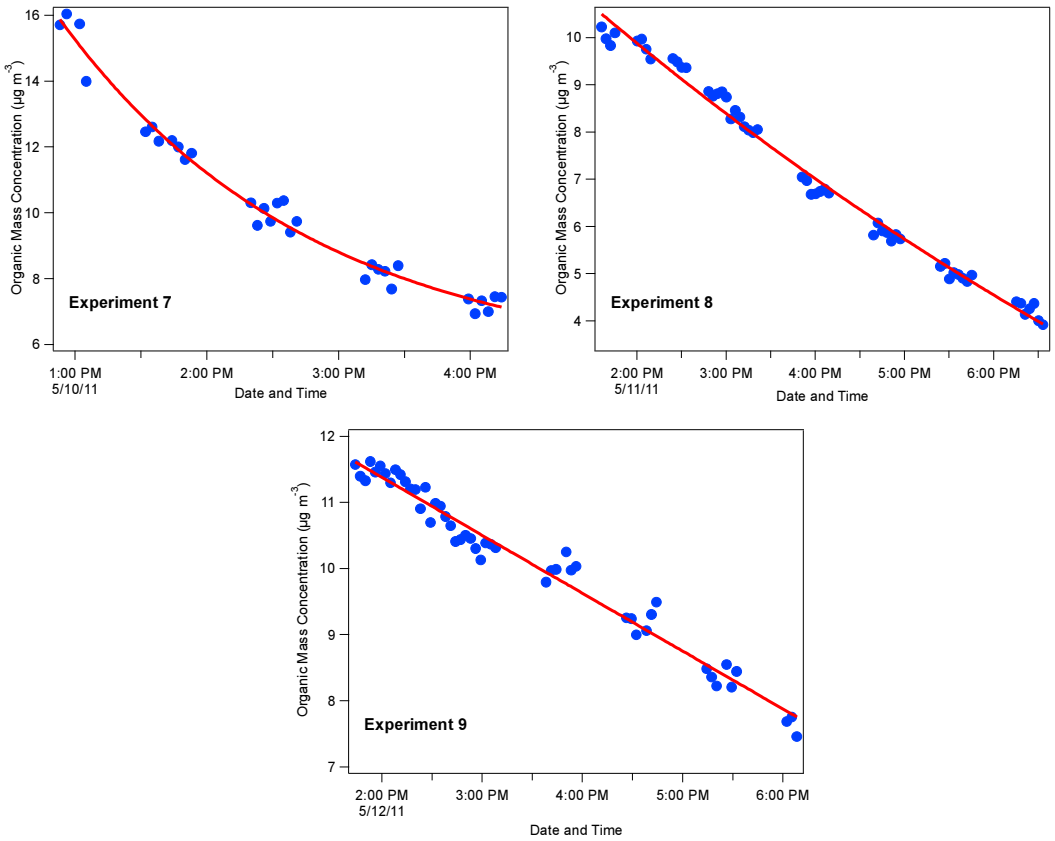

Figure S2. The interpolated fits to the bypass data are shown for each experiment. The blue circles represent the measured organic mass concentration from the bypass line and the red lines represent the interpolated fit, normally an exponential decay.

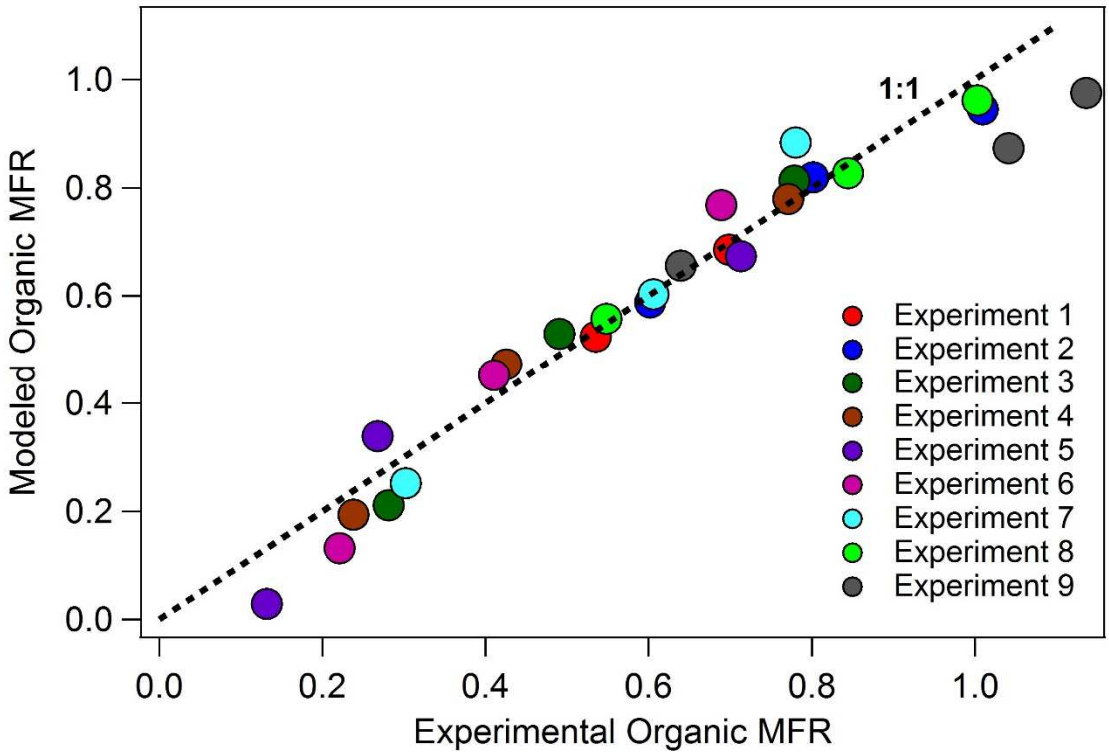

Figure S3. Comparison of the predicted MFRs based on the best fits and the experimental values at 15 s for all temperatures for all experiments.